

Plume formation in strongly temperature-dependent viscosity fluids over a very hot surface

Y. Ke and V. S. Solomatov

Department of Physics, New Mexico State University, Las Cruces, New Mexico 88001

(Received 28 August 2003; accepted 22 December 2003; published online 8 March 2004)

Plume formation in a strongly temperature-dependent viscosity fluid placed on a very hot surface involves an intermediate step—small-scale convection in the thermal boundary layer. We perform numerical simulations and suggest a simple analysis of this process using the stagnant lid convection theory and Canright and Morris' theory of Rayleigh–Taylor instability of two layers with different viscosities. We show that plume formation can approximately be predicted from the requirement that the growth of the large-scale instability becomes faster than the growth of the convecting thermal boundary layer. © 2004 American Institute of Physics. [DOI: 10.1063/1.1648638]

I. INTRODUCTION

Plumes are important features of mantle dynamics on the Earth and other planets. They are thought to be responsible for volcanic “hotspots” such as Hawaii and Yellowstone and for gigantic flood basalt events in the past history of the Earth.^{1–3} They also remove heat from the Earth's interior and provide an efficient cooling of the core which is required for the generation of the magnetic field.⁴ They might play a significant role in global climate and mass extinctions.^{3,5}

Although plume dynamics has been extensively studied in various regimes including high Rayleigh numbers and variable viscosity^{6–11} it is not well understood at very large viscosity contrasts which is relevant to the Earth's mantle. Plumes presumably form as a result of instabilities of the thermal boundary layer at the base of the mantle. A temperature contrast of 1000–2000 K across the thermal boundary layer^{12,13} and a strong dependence of the mantle viscosity on temperature¹⁴ suggest that the viscosity contrast across this boundary layer is larger than 10^4 . It was observed that at such high viscosity contrasts, plume formation involves an intermediate step—small-scale convection in the thermal boundary layer.^{15–18} Previous investigators only reached the critical viscosity when small-scale convection appears but did not investigate this regime. The first stage of plume formation, small-scale convection in the thermal boundary layer, was systematically investigated by Solomatov and Moresi.¹⁹ The goal of this study is to understand the second stage, large-scale instability.

II. MODEL

We consider an idealized two-dimensional box $H \times L$ with the initial temperature $T_0 = 0$. This box is subject to instantaneous heating from below caused by a sudden increase of the bottom temperature from T_0 to $T_b > T_0$ at time $t = 0$. The horizontal and vertical boundaries are free-slip. The side boundaries are thermally insulated.

Convection in a cell with a fixed temperature difference ΔT between the boundaries and with free-slip boundary conditions is described by the following equations:

$$\nabla \cdot \mathbf{u} = 0, \quad (1)$$

$$0 = -\nabla p + \alpha \rho g T \mathbf{n} + \nabla \cdot [\mu (\nabla \mathbf{u} + \{\nabla \mathbf{u}\}^T)], \quad (2)$$

$$\frac{\partial T}{\partial t} + \mathbf{u} \cdot \nabla T = \nabla^2 T, \quad (3)$$

where \mathbf{u} is the velocity vector, T is the temperature, p is the pressure perturbations, α is the thermal expansion, g is the acceleration due to gravity, \mathbf{n} is a unit vector in the direction of gravity, $\kappa = k/\rho c_p$ is the coefficient of thermal diffusion, ρ is the density, k is the thermal conductivity, c_p is the heat capacity at constant pressure, μ is the viscosity, and $\{\}^T$ is the transpose operator. The viscosity is assumed to be an exponential function of temperature:

$$\mu = \mu_0 \exp(-\gamma T), \quad (4)$$

where γ is a constant.

To nondimensionalize the problem, we choose H as the length scale, $t_0 = H^2/\kappa$ as the time scale, and $\Delta T = T_b - T_0$ as the temperature scale. The two nondimensional parameters are the Rayleigh number

$$\text{Ra}_0 = \frac{\alpha \rho_0 g \Delta T H^3}{\kappa \mu_0}, \quad (5)$$

where μ_0 is the viscosity at $T = T_0$, and the parameter

$$\theta = \gamma \Delta T \quad (6)$$

which determines the total viscosity contrast $\exp(\theta)$ across the layer.

To initiate small-scale convection small sinusoidal perturbations are added at the very bottom of the layer. Small-scale convection is not sensitive to the exact perturbation function because the cell size is self-regulated and increases during the growth of the convective boundary layer.¹⁹

Once developed, small-scale convection generates perturbations which, theoretically, can cause large-scale instability and produce a plume. However, at the Rayleigh numbers that we can reach the growth rate of these, very short wavelength perturbations is so small that the convective boundary layer propagates through the entire layer without producing

plumes. Thus, to initiate the large-scale instability, we need to impose large-scale perturbations. An obvious choice would be to use random perturbations and determine the fastest growing mode. However, as we explain later, there is a broad range of wavelengths at which the growth rate is approximately constant. Instead of one fastest growing mode there is a range of modes growing at about the same rate. Under such conditions, the results would be difficult to analyze. Therefore, we systematically investigate the dependence of the growth rate on the wavelength using single mode temperature perturbations:

$$\delta T(x, z) = \epsilon \cos(2\pi x/\lambda) \sin[\pi(1-z)], \quad (7)$$

where $\epsilon=0.001$ is the amplitude of the perturbation and $\lambda=2L$ is the wavelength.

III. NUMERICAL SIMULATIONS

The numerical simulations are performed using the finite element code CITCOM.²⁰ The viscosity contrast is $\exp(\theta)=10^6$. Two values of the Rayleigh number Ra_0 are considered: 3×10^3 and 10^4 . These values are sufficiently high to ensure that the instability occurs when the thickness of the convecting thermal boundary layer is substantially smaller than the thickness of the entire layer (otherwise we would get a different regime in which small-scale convection propagates through the entire layer without generating a plume). On the other hand, these values are low enough to obtain accurate solutions with 128 finite elements in the vertical direction.

The aspect ratio of the numerical domain varies from 0.5×1 to 32×1 (the number of finite elements varies from 64×128 to 4096×128 , respectively). This corresponds to λ from 1 to 64. All cases studied are in the regime in which the characteristic length scale of small-scale convection is much smaller than the length scale of large-scale instabilities. Figure 1 shows an example of plume formation in a 1×1 box for $Ra_0=10^4$. This example clearly shows the development of small-scale convection in the thermal boundary layer followed by plume formation as a result of large-scale instability of the thermal boundary layer. Other cases are very similar and are not shown (besides, cases with large aspect ratios are difficult to visualize).

For the purpose of constraining the onset of plume formation, the simulations need to be run only long enough to reach the initial stage of plume formation. To do so we traced the height d_1 and the growth rate \dot{d}_1 of the convective thermal boundary layer. This interface is defined by an isotherm $T=T_L$. The value of T_L can be chosen as the isotherm $T_L=1-3.7\theta^{-1} \approx 0.73$ defining the boundary of the actively convecting region (θ^{-1} is the scale for the typical temperature variations in the convective region and the coefficient 3.7 is estimated numerically and experimentally in previous studies¹⁹). However, the fluctuations in the position of this isotherm are substantial because of the time-dependent character of small-scale convection. We choose $T_L=0.6$ instead and notice that the results are not very sensitive to the value

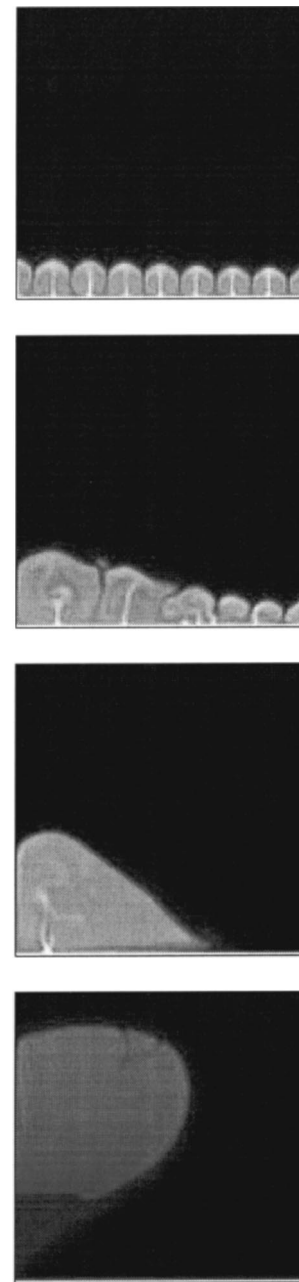


FIG. 1. A sequence of snapshots showing plume formation at large viscosity contrasts in a 1×1 box and $Ra_0=10^4$ (time increases downward).

of T_L as long as it remains within the sharp thermal front just above the convective thermal boundary layer.

We also calculated the growth of the large-scale instability. The amplitude w of the instability is defined as the average separation between the average left half and the average right half positions of the interface. This definition is chosen to minimize the effect of fluctuations (the difference in the positions of the boundary points of the interface turns out to be a less robust definition because of the fluctuations in the convective boundary layer). The growth rate of the instability is defined as \dot{w} . Temporal variations of d_1 and w for 1×1 box are shown in Fig. 2.

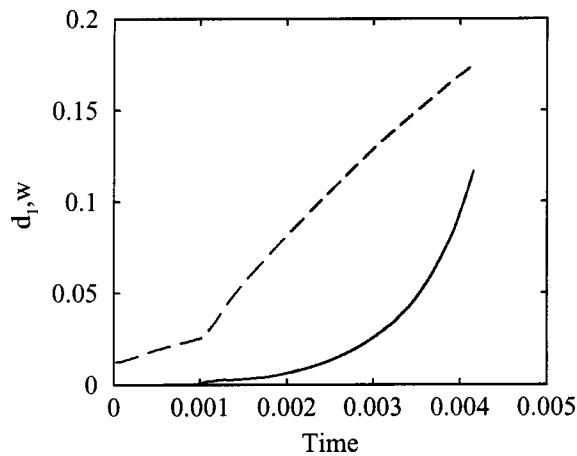


FIG. 2. Thickness, d_1 , of the thermal boundary layer (dashed line) and the amplitude, w , of the large-scale instability (solid line) for the 1×1 case at $Ra_0 = 10^4$. The abrupt increase in the growth rate of the thermal boundary layer is caused by the onset of small-scale convection.

IV. ANALYSIS OF THE NUMERICAL RESULTS

A. Growth of the convective boundary layer

After the onset of small-scale convection, both the bottom heat flux and the growth rate of the convective boundary layer remain approximately constant (Fig. 2)—in agreement with stagnant lid convection theory:¹⁹

$$\dot{d}_1 = \frac{F}{T_1}, \tag{8}$$

where T_1 is the internal temperature of the convective boundary layer.

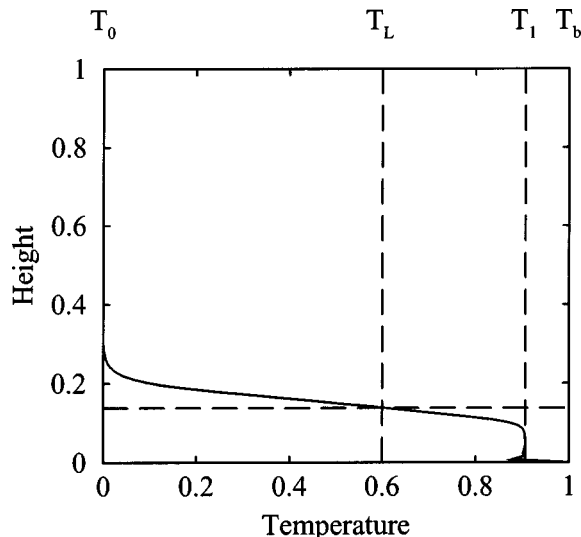


FIG. 3. The temperature profile of the layer. The bottom temperature is $T_b = 1$. The surface temperature is $T_0 = 0$. Temperature in convective region is T_1 . The interface between the upper and lower layers is determined by an isotherm $T = T_L$.

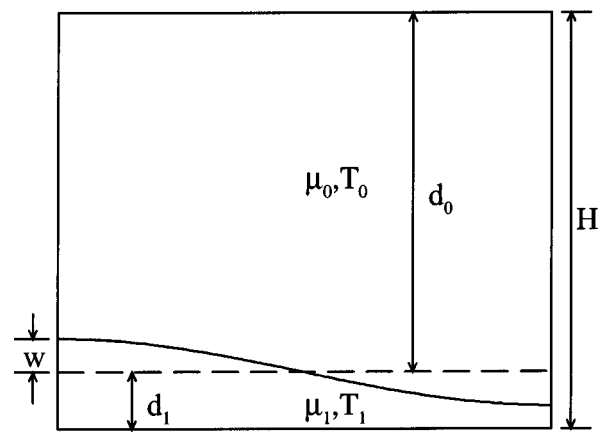


FIG. 4. Interpretation of the large-scale instability in terms of Rayleigh–Taylor instability.

B. Large-scale instability of the thermal boundary layer

The thermally induced density contrast between the convecting boundary layer and the layer above it is the driving force for the large-scale instability of the whole system. It occurs simultaneously with the growth of the convective boundary layer. This process is similar to the Rayleigh–Taylor instability in chemically and rheologically stratified layers.

To interpret the large-scale instability in terms of Rayleigh–Taylor instability consider the thermal structure of the layer in Fig. 3. The temperature profile is characterized by two nearly isothermal regions separated by a sharp interface (this structure was described in detail by Solomatov and Moresi¹⁹). The viscosity of the lower layer can be considered approximately constant because the convective mixing in this region maintains a nearly uniform temperature such that $1 - T_1 \sim \theta^{-1}$ (Ref. 19). In our simulations, $T_1 \approx 0.908$ (independent of the Rayleigh number). The effective viscosity of the lower layer (the convective thermal boundary layer) is $\mu_1 = \mu_0 \exp(-\theta T_1)$. The thickness of the lower layer is d_1 . The upper layer has the temperature $T_0 = 0$ and the viscosity

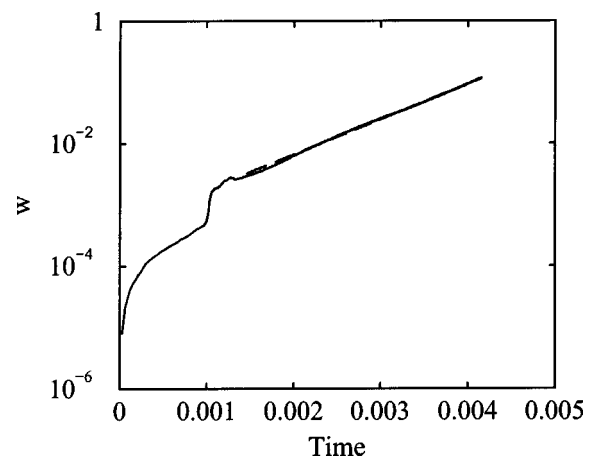


FIG. 5. An example of exponential fit (dashed line) to the growth of the large-scale instability (solid line) (1×1 box, $Ra_0 = 10^4$).

μ_0 which are approximately constant because of the uniform initial conditions. The thickness of the upper layer is $d_0 = 1 - d_1$.

Thus, the large-scale instability can approximately be modeled as a Rayleigh–Taylor instability in a system consisting of two uniform layers (Fig. 4). The viscosity contrast between the layers is $V = \mu_0 / \mu_1$, the thickness ratio is $\beta = d_0 / d_1$ and the (dimensional) density difference between the layers is $\Delta\rho = \alpha\rho_0(T_1 - T_0)$. An important difference between our case and Rayleigh–Taylor instability is that in the latter case the density contrast between the layers is compositional while in our case it is thermal and thus, can, in principle, be eroded by thermal diffusion. However, after the onset of small-scale convection thermal diffusion is unimportant because it becomes much slower than both the growth of the thermal boundary layer and the large-scale instability.

Applying the analytical solution for Rayleigh–Taylor instability of two compositionally distinct layers with different viscosities²¹ to the growth of large-scale instability, we obtain

$$w(t) = w_0 e^{\sigma(t-t_{ss})}, \tag{9}$$

where t_{ss} is the time when small-scale convection starts (when the two-layer structure described above forms), w_0 is the amplitude of the perturbation at $t = t_{ss}$, σ is the growth rate of the instability,

$$\sigma = \frac{Ra_0 V d_0 T_1}{\beta} \tilde{\sigma}, \tag{10}$$

and $\tilde{\sigma}$ is defined as follows:²¹

$$\tilde{\sigma} = \frac{1}{\tilde{k}} \frac{(S - \tilde{K})(c - 1) + V(s - \tilde{k})(C - 1)}{(S - \tilde{K})(s + \tilde{k}) + 2V(Cc - 1 + \tilde{K}\tilde{k}) + V^2(S + \tilde{K})(s - \tilde{k})}, \tag{11}$$

where $\tilde{k} \equiv 2kd_1$, $\tilde{K} \equiv 2kd_0$, $c \equiv \cosh(\tilde{k})$, $C \equiv \cosh(\tilde{K})$, $s \equiv \sinh(\tilde{k})$, $S \equiv \sinh(\tilde{K})$, and $k \equiv 2\pi/\lambda$ is the wave number.

The growth rate depends on three dimensionless parameters: the viscosity contrast V , the thickness ratio β , and the nondimensional wave number \tilde{k} . Canright and Morris' analysis²¹ of the above equation shows that for $\beta \gg 1$ and $V \gg \beta^3$ (which applies to our case) there is a plateau, $(\beta/V)^{1/2} \ll \tilde{k} \ll \beta^{-1}$, where the growth rate of perturbations is almost independent of the wave number:

$$\tilde{\sigma} \approx \frac{\beta}{4V}. \tag{12}$$

Assuming that $\gamma \gg 1$ so that $T_1 \approx 1$, we obtain

$$\sigma \approx \frac{1}{4} Ra_0. \tag{13}$$

It is interesting to note that in this regime the large-scale instability is controlled by the viscous stresses in the upper layer and is not affected by the dynamics of the lower layer.

Figures 5 and 6 show a good agreement between the theoretical predictions and the numerical simulations. They also show that in agreement with the theory, instead of a sharp peak, there is a broad plateau where the dependence on the wave number is very weak.

C. Onset of plume formation

Eventually the thickness of the convecting boundary layer reaches a critical value at which the large-scale instability becomes faster than the growth rate of the convecting boundary layer and the system becomes unstable. This time is defined as the onset time, t_{pl} , of plume formation and is calculated from the requirement that

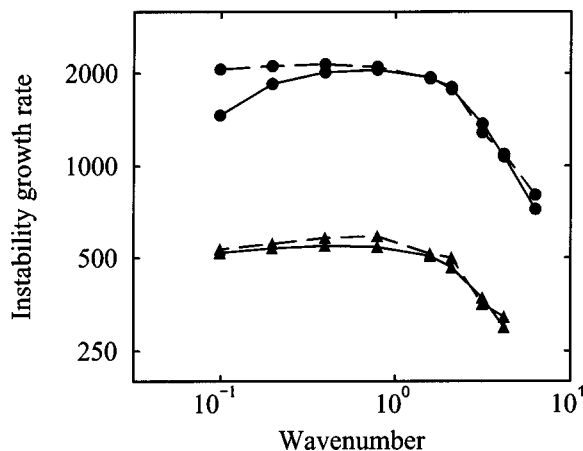


FIG. 6. Theoretical predictions (solid lines) versus numerical results (dashed lines) for the instability growth rate as a function of wave number. Triangles correspond to $Ra = 3 \times 10^3$; circles correspond to $Ra = 10^4$.

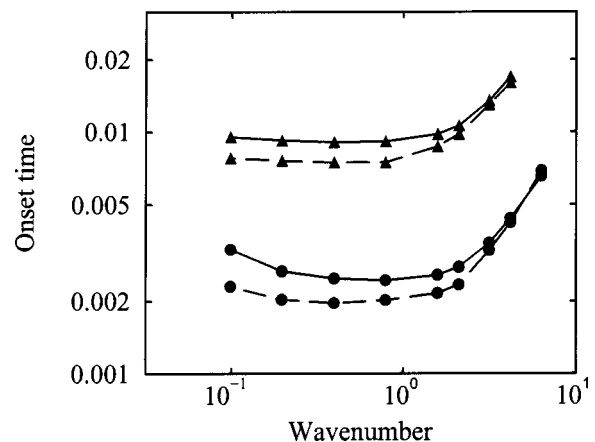


FIG. 7. Theoretical predictions (solid lines) versus numerical results (dashed lines) for the growth rate of large-scale instability. Triangles correspond to $Ra = 3 \times 10^3$; circles correspond to $Ra = 10^4$.

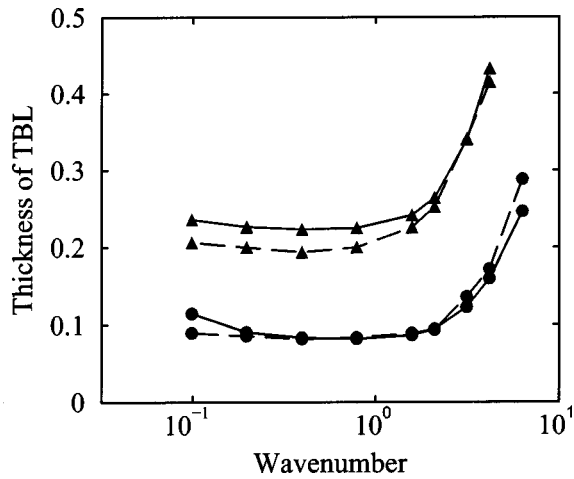


FIG. 8. Theoretical predictions (solid lines) versus numerical results (dashed line) for the thickness of the thermal boundary layer at the onset time of plume formation. Triangles indicate $Ra=3 \times 10^3$; circles indicate $Ra=10^4$.

$$\dot{w} = \dot{d}_1. \tag{14}$$

Since $\dot{w} = w_0 \sigma e^{\sigma(t-t_{ss})}$ we obtain

$$t_{pl} = t_{ss} + \frac{\ln(\delta_0/w_0)}{\sigma}, \tag{15}$$

where

$$\delta_0 = \frac{F}{\sigma T_1}. \tag{16}$$

The thickness of the thermal boundary layer at the onset time is

$$\delta_{pl} = 0.74 t_{ss}^{1/2} + \frac{F}{T_1} (t_{pl} - t_{ss}), \tag{17}$$

where the coefficient 0.74 is the theoretical coefficient calculated from the conductive growth of the thermal boundary layer whose boundary is defined by the isotherm $T = T_L$.

The theoretical predictions for the time t_{pl} , Eq. (15), and the thermal boundary layer thickness δ_{pl} at the onset of plume formation, Eq. (17), with σ defined by Eqs. (10)–(11) are in good agreement with the numerical results (Figs. 7 and 8).

V. CONCLUSION

We performed numerical simulations of plume formation in the regime of very large viscosity contrasts. In this regime, plumes form after an extended period of small-scale convection in the thermal boundary layer. A simple analysis based on the stagnant lid convection theory¹⁹ and the Rayleigh–Taylor instability theory²¹ suggests that plume formation can approximately be described as a Rayleigh–Taylor instability

of the two-layer system consisting of the vigorously convecting thermal boundary layer and a nearly isothermal layer above it. Plumes form when the growth rate of the large-scale instability of this two-layer system exceeds the growth rate of the convective thermal boundary layer. In the future it would be very interesting to investigate plume formation caused by perturbations associated with small-scale convection itself. This is a challenging problem which involves a strong interaction between the two scales of convection.

¹W. J. Morgan, “Convection plumes in the lower mantle,” *Nature (London)* **230**, 42 (1971).
²M. A. Richards, R. A. Duncan, and V. E. Courtillot, “Flood basalts and hot-spot tracks-plume heads and tails,” *Science* **246**, 103 (1989).
³D. E. Loper, “Mantle plumes and their effect on the Earth’s surface: A review and synthesis,” *Dyn. Atmos. Oceans* **27**, 35 (1998).
⁴D. J. Stevenson, T. Spohn, and G. Schubert, “Magnetism and thermal evolution of the terrestrial planets,” *Icarus* **54**, 466 (1983).
⁵P. R. Renne, Z. C. Zhang, M. A. Richards, M. T. Black, and A. R. Basu, “Synchrony and causal relations between Permian–Triassic boundary crises and Siberian flood volcanism,” *Science* **269**, 1413 (1995).
⁶R. W. Griffiths, “Thermals in extremely viscous fluids, including the effects of temperature-dependent viscosity,” *J. Fluid Mech.* **166**, 115 (1986).
⁷D. E. Loper and F. D. Stacey, “The dynamical and thermal structure of deep mantle plumes,” *Phys. Earth Planet. Inter.* **33**, 304 (1983).
⁸C. Lithgow-Bertelloni, M. A. Richards, C. P. Conrad, and R. W. Griffiths, “Plume generation in natural thermal convection at high Rayleigh and Prandtl numbers,” *J. Fluid Mech.* **434**, 1 (2001).
⁹U. Hansen, D. Yuen, and S. E. Kroening, “Transition to hard turbulence in thermal convection at infinite Prandtl number,” *Phys. Fluids A* **2**, 2157 (1990).
¹⁰M. Manga, D. Weeraratne, and S. J. S. Morris, “Boundary-layer thickness and instabilities in Benard convection,” *Phys. Fluids* **13**, 802 (2001).
¹¹M. Manga and D. Weeraratne, “Experimental study of non-Boussinesq Rayleigh–Benard convection at high Rayleigh and Prandtl numbers,” *Phys. Fluids* **11**, 2969 (1999).
¹²Q. Williams, “The temperature contrast across D,” in *The Core–Mantle Boundary Region, Geodynamics Series*, edited by M. Gurnis, M. E. Wyssession, E. Knittle, and B. A. Buffett (AGU, Washington, D.C., 1998), Vol. 28, pp. 73–81.
¹³R. Boehler, “High-pressure experiments and the phase diagram of lower mantle and core materials,” *Rev. Geophys.* **38**, 221 (2000).
¹⁴D. Yamazaki and S.-I. Karato, “Some mineral physics constraints on the rheology and geothermal structure of Earth’s lower mantle,” *Am. Mineral.* **86**, 385 (2001).
¹⁵D. A. Yuen and W. R. Peltier, “Mantle plumes and the thermal stability of the D” layer,” *Geophys. Res. Lett.* **7**, 625 (1980).
¹⁶U. Christensen, “Instability of a hot boundary layer and initiation of thermochemical plumes,” *Ann. Geophys.* **2**, 311 (1984).
¹⁷P. Olson, G. Schubert, and C. Anderson, “Plume formation in the D”-layer and the roughness of the core–mantle boundary,” *Nature (London)* **327**, 409 (1987).
¹⁸P. E. Thompson and P. J. Tackley, “Generation of mega-plumes from the core–mantle boundary in a compressible mantle with temperature-dependent viscosity,” *Geophys. Res. Lett.* **25**, 1999 (1998).
¹⁹V. S. Solomatov and L.-N. Moresi, “Small-scale convection in the D” layer,” *J. Geophys. Res.* **107** (2002), doi:10.1029/2000JB000063.
²⁰L.-N. Moresi and V. S. Solomatov, “Numerical investigation of 2D convection with extremely large viscosity variations,” *Phys. Fluids* **7**, 2154 (1995).
²¹D. Carrighr and S. Morris, “Buoyant instability of a viscous film over a passive fluid,” *J. Fluid Mech.* **255**, 349 (1993).